Supplementary Information

Mononuclear nickel(II)-superoxo and nickel(III)-peroxo complexes bearing a common macrocyclic TMC ligand

Jaeheung Cho,[a,b] Hye Yeon Kang,[a] Lei V. Liu,[c] Ritimukta Sarangi,[d] Edward I. Solomon,[c,d] and Wonwoo Nam*[a]

[a]*Department of Bioinspired Science, Ewha Womans University, Seoul 120–750, Korea.*
[b]*Department of Emerging Materials Science, DGIST, Daegu 711-873, Korea.*
[c]*Department of Chemistry, Stanford University, Stanford, California 94305, USA*
[d]*Stanford Synchrotron Radiation Lightsource, SLAC National Accelerator Laboratory, Stanford University, Menlo Park, California 94025-7015, USA*

*To whom correspondence should be addressed.
E-mail: wwnam@ewha.ac.kr

Experimental Section

Materials and Instrumentation. All chemicals obtained from Aldrich Chemical Co. were the best available purity and used without further purification unless otherwise indicated. Solvents were dried according to published procedures and distilled under Ar prior to use.[1] $H_2^{18}O_2$ (95% ^{18}O-enriched, 2% $H_2^{18}O_2$ in water) was purchased from ICON Services Inc. (Summit, NJ, USA). The 13-TMC (1,4,7,10-tetramethyl-1,4,7,10-tetraazacyclotridecane) was prepared by reacting excess amount of formaldehyde and formic acid with 1,4,7,10-tetraazacyclotridecane.[2]

UV-vis spectra were recorded on a Hewlett Packard 8453 diode array spectrophotometer equipped with a UNISOKU Scientific Instruments for low-temperature experiments or with a circulating water bath. Electrospray ionization mass spectra (ESI-MS) were collected on a Thermo Finnigan (San Jose, CA, USA) LCQ^{TM} Advantage MAX quadrupole ion trap instrument, by infusing samples directly into the source using a manual method. The spray voltage was set at 4.2 kV and the capillary temperature at 80 °C. Resonance Raman (rR) spectra were obtained using a triple monochromator (Spex 1877 CP) with 1200, 1800, and 2400 grooves/mm holographic spectrograph gratings and an Andor Newton CCD detector cooled to −80 °C. Excitation was provided by Ar (Innova Sabre 25/7) ion lasers with incident power of ~20 mW using an ~135° backscattering configuration. All measurements were carried out at 77 K. Raman shifts were calibrated with citric acid. The spectral resolution was ~2 cm^{-1}. CW-EPR spectra were taken at 5 K using an X-band Bruker EMX-plus spectrometer equipped with a dual mode cavity (ER 4116DM). Low temperatures were achieved and controlled using an Oxford Instruments ESR900 liquid He quartz cryostat with an Oxford Instruments ITC503 temperature and gas flow controller. Product analysis was performed with an Agilent Technologies 6890N gas chromatograph (GC) and Thermo Finnigan (Austin, Texas, USA) FOCUS DSQ (dual stage quadrupole) mass spectrometer interfaced with Finnigan FOCUS gas chromatograph (GC-MS). ^{31}P and ^{1}H NMR spectra were measured with Bruker DPX-400 spectrometer.

Synthesis and Characterization of [Ni^{II}(13-TMC)(CH$_3$CN)](ClO$_4$)$_2$ (1-(ClO$_4$)$_2$). 13-TMC (0.5 g, 2.06 mmol) was added to an acetonitrile solution (50 mL) of Ni(ClO$_4$)$_2$·6H$_2$O (0.91 g, 2.48 mmol). The mixture was refluxed for 12 h, affording a blue solution. After the mixture cooled to room temperature, the solvent was removed under vacuum to give a blue solid, which was collected by filtration and washed with methanol several times to remove the remaining Ni(ClO$_4$)$_2$·6H$_2$O. Yield: 0.82 g (74%). UV-vis (CH$_3$CN) (see ESI†, Fig. S1,): λ_{max} (ε) = 375 nm (160 M^{-1} cm^{-1}), 575 nm (60 M^{-1} cm^{-1}), and 720 nm (20 M^{-1} cm^{-1}). ESI-MS (CH$_3$CN) (see ESI†, Fig. S2): m/z 150.2 for [Ni(13-TMC)]$^{2+}$, 170.3 for [Ni(13-TMC)(CH$_3$CN)]$^{2+}$, and 399.3 for [Ni(13-TMC)(ClO$_4$)]$^{+}$. X-ray crystallographically suitable crystals were obtained by slow diffusion of Et$_2$O into a solution of the complex in CH$_3$CN.

Generation and Characterization of [Ni^{II}(13-TMC)(O$_2$)]$^{+}$ (2). Treatment of **1** (2 mM) with 2 equiv. of H$_2$O$_2$ in the presence of 1.3 equiv. of tetramethylammonium hydroxide (TMAH) in CH$_3$CN (2 mL)

afforded the formation of a yellow green solution at –40 ºC. Spectroscopic data, including UV-vis, resonance Raman, and EPR, were reported in Fig. 1. $[Ni^{II}(13\text{-TMC})(^{18}O_2)]^+$ was prepared by adding 2 equiv. of $H_2^{18}O_2$ (14 μL, 90% ^{18}O-enriched, 2% $H_2^{18}O_2$ in water) in the presence of 1.3 equiv. of TMAH in CH_3CN at –40 ºC.

Generation and Characterization of $[Ni^{III}(13\text{-TMC})(O_2)]^+$ (3). Treatment of **1** (4 mM) with 10 equiv. of H_2O_2 in the presence of 2 equiv. of triethylamine (TEA) in CH_3CN (2 mL) afforded the formation of a green solution at 25°C. Spectroscopic data, including UV-vis, ESI-MS, resonance Raman, and EPR, were reported in Fig. 2. $[Ni^{III}(13\text{-TMC})(^{18}O_2)]^+$ was prepared by adding 10 equiv. of $H_2^{18}O_2$ (138 μL, 90% ^{18}O-enriched, 2% $H_2^{18}O_2$ in water) to a solution containing **1** (4 mM) and 2 equiv. of TEA in CH_3CN (2mL) at ambient temperature. X-ray crystallographically suitable crystals were obtained by slow diffusion of Et_2O into a solution of the complex in CH_3CN.

Reactivity Studies. All reactions were run monitoring UV-vis spectral changes of reaction solutions, and rate constants were determined by fitting the changes in absorbance at 331 nm for $[Ni^{II}(13\text{-TMC})(O_2)]^+$ (**2**) and 413 nm for $[Ni^{III}(13\text{-TMC})(O_2)]^+$ (**3**). Reactions were run at least in triplicate, and the data reported represent the average of these reactions. *In situ*-generated **2** and **3** were used in kinetic studies, such as the oxidation of triethylphosphine (PEt_3) in CH_3CN/CH_3OH (1:1) at –40 ºC and 2-phenylpropionaldehyde (2-PPA) in CH_3CN at 25 °C, respectively. After the completion of reactions, pseudo-first-order fitting of the kinetic data allowed us to determine k_{obs} values. Products formed in the oxidation of PEt_3 by **2** in CH_3CN/CH_3OH (1:1) at –40 ºC were analyzed by ^{31}P and ^1H NMR spectroscopy. Quantitative analysis was made on the basis of comparison of ^{31}P and ^1H NMR peak integration between products and authentic samples. $OPEt_3$ was formed as a sole product in the oxidation of PEt_3 by **2**. Products formed in the oxidation of 2-PPA by **3** in CH_3CN at 25 °C were analyzed by GC and GC-MS. The purity of substrates was checked with GC and GC-MS prior to use. Products were analyzed by injecting the reaction mixture directly into GC and GC-MS. Products were identified by comparing with authentic samples, and product yields were determined by comparison against standard curves prepared with authentic samples and using decane as an internal standard.

X-ray Crystallography. Single crystals of **1**-$(ClO_4)_2$ and **3**-$(ClO_4)·CH_3CN$ were picked from solutions by a nylon loop (Hampton Research Co.) on a hand made copper plate mounted inside a liquid N_2 Dewar vessel at *ca*. –40 ºC and mounted on a goniometer head in a N_2 cryostream. Data collections were carried out on a Bruker SMART APEX II CCD diffractometer equipped with a monochromator in the Mo Kα ($\lambda = 0.71073$ Å) incident beam. The CCD data were integrated and scaled using the Bruker-SAINT software package, and the structure was solved and refined using SHELXTL V 6.12.[3] Hydrogen atoms were located in the calculated positions for **3**-$(ClO_4)·CH_3CN$. However, hydrogen atoms could not be placed in ideal position for **1**-$(ClO_4)_2$, due to the high degree of disorder. Crystal data for **1**-$(ClO_4)_2$:

$C_{15}Cl_2NiN_5O_8$, Tetragonal, *P4/nmm*, Z = 2, *a* = 9.2584(6), *b* = 9.2584(6), *c* = 14.1473(17) Å, *V* = 1212.68(18) Å^3, μ = 1.065 mm^{-1}, ρ_{calcd} = 1.391 g/cm^3, R$_1$ = 0.0612, wR$_2$ = 0.1594 for 912 unique reflections, 75 variables. Crystal data for **3**-(ClO$_4$)·CH$_3$CN: $C_{15}H_{33}ClNiN_5O_6$, Monoclinic, *Pc*, Z = 2, *a* = 7.7299(2), *b* = 7.7263(2), *c* = 17.8514(5) Å, β = 100.673(2)^o, *V* = 1047.70(5) Å^3, μ = 1.095 mm^{-1}, ρ_{calcd} = 1.501 g/cm^3, R$_1$ = 0.0360, wR$_2$ = 0.0762 for 3604 unique reflections, 258 variables. The crystallographic data for **1**-(ClO$_4$)$_2$ and **3**-(ClO$_4$)·CH$_3$CN are listed in Table S1, and Table S2 lists the selected bond distances and angles. CCDC-729199 for **1**-(ClO$_4$)$_2$ and -900983 for **3**-(ClO$_4$)·CH$_3$CN contain the supplementary crystallographic data for this paper. These data can be obtained free of charge via www.ccdc.cam.ac.uk/data_request/cif (or from the Cambridge Crystallographic Data Centre, 12, Union Road, Cambridge CB2 1EZ, UK; fax: (+44) 1223-336-033; or deposit@ccdc.cam.ac.uk).

X-ray Absorption Spectroscopy. The Ni K-edge X-ray absorption spectra of **2** and **3** were measured at the Stanford Synchrotron Radiation Laboratory (SSRL) on the unfocussed 20-pole 2 T wiggler side-station beam line 7-3 under standard ring conditions of 3 GeV and ~100 mA. A Si(220) double crystal monochromator was used for energy selection. A Rh-coated harmonic rejection mirror was used on beam line 7-3 to reject components of higher harmonics. The solution samples for **2** and **3** (~120 µL) were transferred into 2 mm delrin XAS cells with 37 µm Kapton tape windows under synthesis conditions. The samples were immediately frozen after preparation and stored under liquid N$_2$. During data collection, the samples were maintained at a constant temperature of 10 K using an Oxford Instruments CF 1208 liquid helium cryostat. Data were measured to *k*=15 Å^{-1} on **2** and **3** (fluorescence mode) using a Canberra Ge 30-element array detector. Internal energy calibration was accomplished by simultaneous measurement of the absorption of a Ni-foil placed between two ionization chambers situated after the sample. The first inflection point of the foil spectrum was fixed at 8331.6 eV. Data presented here are 16-scan (**2**) and 17-scan (**3**) average spectra, which were processed by fitting a second-order polynomial to the pre-edge region and subtracting this from the entire spectrum as background. A four-region spline of orders 2, 3, 3 and 3 was used to model the smoothly decaying post-edge region. The data were normalized by subtracting the cubic spline and assigning the edge jump to 1.0 at 8320 eV using the Pyspline program.[4]

Theoretical EXAFS signals $\chi(k)$ were calculated by using *FEFF* (macintosh version 8.4)[5-7] on the crystal of **3**. Starting from the structure of **3**, structural models for **2** were generated using Avogadro.[8] Theoretical models were fit to the data using EXAFSPAK.[9] The structural parameters varied during the fitting process were the bond distance (R) and the bond variance σ^2, which is related to the Debye-Waller factor resulting from thermal motion, and static disorder of the absorbing and scattering atoms. The non-structural parameter E$_0$ (the energy at which *k*=0) was also allowed to vary but was restricted to a common value for every component in a given fit. Coordination numbers was systematically varied in the course of the fit but were fixed within a given fit. A comparison of the k^3 weighted Ni K-edge EXAFS for

1 and **2** along with their non-phase shift corrected Fourier transforms (k=2-14 Å^{-1}) is shown in Fig. 5a. *FEFF* fits to the data are presented in Figs. 5b and 5c and Tables S4 and S5. The second and third shells of the EXAFS data were fit with single and multiple-scattering contributions from the 13-TMC ligand.

Density Functional Theory Calculations. Gradient-corrected, (GGA) spin-unrestricted, broken-symmetry, density functional calculations were carried out using the ORCA[10,11] package on an 12-cpu linux cluster. The Becke88[12,13] exchange and Perdew86[14] correlation non-local functionals were employed to compare the electronic and geometric structure differences between **2** and **3**. The B3LYP[12,13,15] functional was also tested but was not used since it predicted an incorrect (Ni^{II}-superoxide) ground state for **3**. The coordinates obtained from the crystal structure of **3** were used as the starting input structure. For **2**, the crystal structure of **3** was modified to an η^1-O$_2$ binding mode and used as the starting input structure.

The core properties basis set CP(PPP)[16] (as implemented in ORCA) was used on Ni and the Ahlrichs' all electron triple-ζ TZVP[17,18] basis set was used on all other atoms. A tight convergence criterion was selected. Population analyses were performed by means of Mulliken Population Analysis (MPA).[19] Wave functions were visualized and orbital contour plots were generated in Molden.[20] Compositions of molecular orbitals and overlap populations between molecular fragments were calculated using the QMForge.[4] Select DFT parameters are tabulated in Table S6.

Since the orientation of the four methyl groups on the 13-TMC ligand is not known for **2**, DFT calculations were performed to test all probable orientations (Table S7). The calculations show that only the *4s* (all methyl groups *syn*) and *3s1a* (3 methyl groups are *syn* and 1 methyl group is *anti*) geometries are energetically favorable. However, while the Ni-O distance in *4s* agrees well with the EXAFS data, the theoretical distance in *3s1a* is inconsistent with experiment. This, shows that **2** has the *4s* orientation (same as **3**). The EXAFS data indicate the presence of a weakly coordinated ligand at 2.17 Å. This could indicate trans-axial Ni-N(MeCN) ligation. However, DFT optimizations with a trans-axial MeCN or water moved the molecule beyond coordination distance to Ni (>4 Å). Optimizations with the Ni-N/O distances restricted at 2.2 Å, resulted in energies significantly higher (>20 kcal/mol).

References

[1]   *Purification of Laboratory Chemicals*; W. L. F. Armarego and D. D. Perrin, Eds.; Pergamon Press: Oxford, 1997.

[2]   J. A. Halfen and V. G. Young, Jr., *Chem. Commun.* **2003**, 2894-2895.

[3]   G. M. Sheldrick, *SHELXTL/PC*. Version 6.12 for Windows XP. 2001, Bruker AXS Inc., Madison, Wisconsin, USA.

[4]   A. Tenderholt, *Pyspline and QMForge*, 2007.

[5]   J. Mustre de Leon, J. J. Rehr, S. I. Zabinsky and R. C. Albers, *Phys. Rev. B: Condens. Matter* **1991**, *44*, 4146-4156.

[6]   J. J. Rehr and R. C. Albers, *Rev. Mod. Phys.* **2000**, *72*, 621-654.

[7]   J. J. Rehr, J. Mustre de Leon, S. I. Zabinsky and R. C. Albers, *J. Am. Chem. Soc.* **1991**, *113*, 5135-5140.

[8]   Avogadro: an open-source molecular builder and visualization tool. Version 1.XX. http://avogadro.openmolecules.net/.

[9]   G. N. George, *EXAFSPAK and EDG-FIT*, 2000.

[10]   F. Neese, *ORCA: An Ab initio, DFT and Semiempirical Electronic Structure Package.*, Version 2.6.35, 2008.

[11]   F. Neese and G. Olbrich, *Chem. Phys. Lett.* **2002**, *362*, 170-178.

[12]   A. D. Becke, *Phys. Rev. A* **1988**, *38*, 3098-3100.

[13]   A. D. Becke, *J. Chem. Phys.* **1993**, *98*, 5648-5652.

[14]   J. P. Perdew, *Phys. Rev. B* **1986**, *33*, 8822-8824.

[15]   C. T. Lee, W. T. Yang and R. G. Parr, *Phys. Rev. B* **1988**, *37*, 785-789.

[16]   S. Sinnecker, L. D. Slep, E. Bill and F. Neese, *Inorg. Chem.* **2005**, *44*, 2245-2254.

[17]   A. Schaefer, H. Horn and R. Ahlrichs, *J. Chem. Phys.* **1992**, *97*, 2571-2577.

[18]   A. Schaefer, C. Huber and R. Ahlrichs, *J. Chem. Phys.* **1994**, *100*, 5829-5835.

[19]   R. S. Mulliken, *J. Chem. Phys.* **1955**, *23*, 1831-1833.

[20]   G. Schaftenaar and J. H. Noordik, *J. Comput-Aided. Mol. Des.* **2000**, *14*, 123-134.

Table S1. Crystal Data and Structure Refinements for **1**-(ClO$_4$)$_2$ and **3**-(ClO$_4$)·CH$_3$CN.

	1-(ClO$_4$)$_2$	**3**-(ClO$_4$)·CH$_3$CN
Empirical formula	C$_{15}$Cl$_2$NiN$_5$O$_8$	C$_{15}$H$_{33}$ClNiN$_5$O$_6$
Formula weight	507.81	473.62
Temperature (K)	170	100
Wavelength (Å)	0.71073	0.71073
Crystal system/space group	Tetragonal, *P4/nmm*	Monoclinic, *Pc*
Unit cell dimensions		
a (Å)	9.2584(6)	7.7299(2)
b (Å)	9.2584(6)	7.7263(2)
c (Å)	14.1473(17)	17.8514(5)
α (º)	90.00	90.00
β (º)	90.00	100.673(2)
γ (º)	90.00	90.00
Volume (Å^3)	1212.68(18)	1047.70(5)
Z	2	2
Calculated density (g/cm^{-3})	1.391	1.501
Absorption coefficient (mm^{-1})	1.065	1.095
Reflections collected	7472	8344
Independent reflections [R(int)]	912 [0.0619]	3604 [0.0407]
Refinement method	Full-matrix least-squares on F^2	Full-matrix least-squares on F^2
Data/restraints/parameters	912/0/75	3604/2/258
Goodness-of-fit on F^2	1.002	0.980
Final R indices [$I > 2$sigma(I)]	$R_1 = 0.0612$, $wR_2 = 0.1594$	$R_1 = 0.0360$, $wR_2 = 0.0762$
R indices (all data)	$R_1 = 0.0815$, $wR_2 = 0.1651$	$R_1 = 0.0445$, $wR_2 = 0.0801$
Largest difference peak and hole (e/Å^3)	0.612 and −0.384	0.362 and −0.294

Table S2. Selected Bond Distances (Å) and Angles (°) for **1**-(ClO$_4$)$_2$ and **3**-(ClO$_4$)·CH$_3$CN.

Bond Distances (Å)			
1-(ClO$_4$)$_2$		**3**-(ClO$_4$)·CH$_3$CN	
Ni1-N1	2.082(4)	Ni1-N1	2.046(3)
Ni1-N2	1.989(8)	Ni1-N2	2.192(3)
		Ni1-N3	2.076(3)
		Ni1-N4	2.210(3)
		Ni1-O1	1.897(3)
		Ni1-O2	1.898(3)
		O1-O2	1.383(4)

Bond Angles (°)			
1-(ClO$_4$)$_2$		**3**-(ClO$_4$)·CH$_3$CN	
N1- Ni1-N2	101.54(13)	N1-Ni1-N2	82.32(13)
		N1-Ni1-N3	118.25(13)
		N1-Ni1-N4	83.79(13)
		N2-Ni1-N3	83.86(12)
		N2-Ni1-N4	162.54(11)
		N3-Ni1-N4	93.51(12)
		O1-Ni1-O2	42.73(12)
		Ni1-O1-O2	68.69(16)
		Ni1-O2-O1	68.58(16)

Table S3. Ni-K Pre-edge Analysis.

	Pre-edge (1s→3d) (eV)[a]	Ni K rising-edge (eV)[b]
2	8331.6(0.02)[c]	8341.4
3	8332.3(0.02)	8341.7

[a]Intensity weighted average energy of pre-edge multiplet features. [b]Energy position at 0.5 intensity. [c]Values in parentheses are the statistical standard deviations calculated from the individual acceptable fits used in the analysis. Fits performed using Edg-Fit (a peak fitting routine in EXAFSPAK, reference 6)

Table S4. EXAFS Least Squares Fitting Results for **2**.

Fit	Coordination/Path	R(Å)^a	$\sigma^2(\text{Å}^2)^b$	E_0 (eV)	F^c
Fit1 Shown in Figure 5B	1 Ni-O	1.90	684	1.59	0.137
	4 Ni-N	2.07	494		
	1 Ni-N	2.17	135		
	4 Ni-C	2.87	314		
	4 Ni-C^d	3.02	/314		
	12 Ni-C-N^d	3.19	/314		
	16 Ni-C-N^d	3.23	/314		
Fit2	1 Ni-O	1.91	176	1.97	0.143
	5 Ni-N	2.10	164		
	4 Ni-C	2.87	330		
	4 Ni-C^d	3.03	/330		
	12 Ni-C-N^d	3.19	/330		
	16 Ni-C-N^d	3.25	/330		

^{a}The estimated standard deviations for the distances are in the order of ± 0.02 Å. ^{b}The σ^2 values are multiplied by 10^5. ^{c}Error is given by $\Sigma[(\chi_{obsd} - \chi_{calcd})^2 k^6]/\Sigma[(\chi_{obsd})^2 k^6]$. ^{d}/ indicates the σ^2 value for the path is linked to the preceding path. The S_0^2 factor was set at 1.1.

Table S5. EXAFS Least Squares Fitting Results for **3**.

Fit	Coordination/Path	$R(\text{Å})^a$	$\sigma^2(\text{Å}^2)^b$	E_0 (eV)	F^c
Fit1 Shown in Figure 5B	2 Ni-O	1.89	455	2.47	0.138
	2 Ni-N	2.05	216		
	2 Ni-N	2.16	216		
	4 Ni-C	2.84	501		
	4 Ni-C^d	3.02	/501		
	8 Ni-C-N^d	3.08	/501		
	16 Ni-C-N^d	3.26	/501		
Fit2	1 Ni-O	1.90	513	2.68	0.144
	4 Ni-N	2.10	726		
	4 Ni-C	2.85	517		
	4 Ni-C^d	3.01	/517		
	8 Ni-C-N^d	3.08	/517		
	16 Ni-C-N^d	3.26	/517		

^{a}The estimated standard deviations for the distances are in the order of $\pm\ 0.02$ Å. ^{b}The σ^2 values are multiplied by 10^5. ^{c}Error is given by $\Sigma[(\chi_{obsd} - \chi_{calcd})^2 k^6]/\Sigma[(\chi_{obsd})^2 k^6]$. ^{d}/ indicates the σ^2 value for the path is linked to the preceding path. The S_0^2 factor was set at 1.1.

Table S6. Selected DFT Parameters.

Model	Structural Parameters					Mayer Bond Order		Mulliken Spin-Density
	Ni-$O_1(O_2)$	O_1-O_2	Ni-N_1[a]	Ni-N_2[a]	NiO_1O_2	Ni-$O_1(O_2)$	O-O	Ni, O_1, O_2
2	1.946 (2.837)	1.322	2.13	2.14	119.3°	0.75(0.33)	1.15	1.32, -0.35, -0.21
3	1.902 (1.903)	1.388	2.13	2.23	68.6°	0.81(0.80)	0.88	0.81, -0.06, 0.00

[a]Average of the two trans Ni-N distances.

Table S7. DFT Calculations for Four Methyl Group Orientation Prediction in **2**.

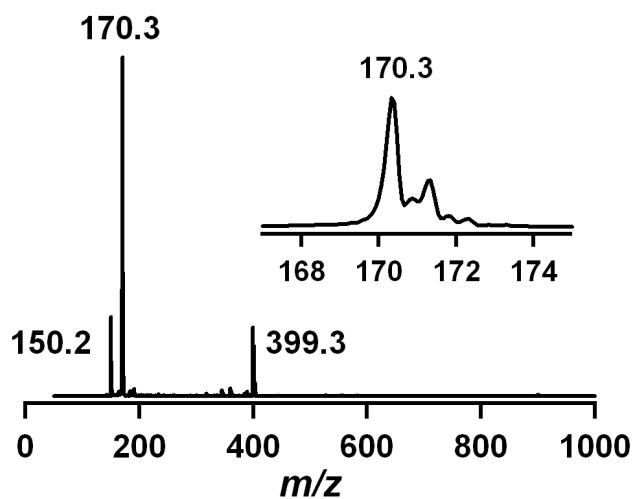|	4u	2u2d[a]	3u1td	4d
Energy	-1.83	10.95	-1.73	14.05
Ni-O	1.95	2.0	1.82	2.1
EXAFS correlation	Good	Bad	Bad	Bad

[a]'u' and 'd' refer to *syn* and *anti* position of the methyl groups relative to the O_2 moiety.

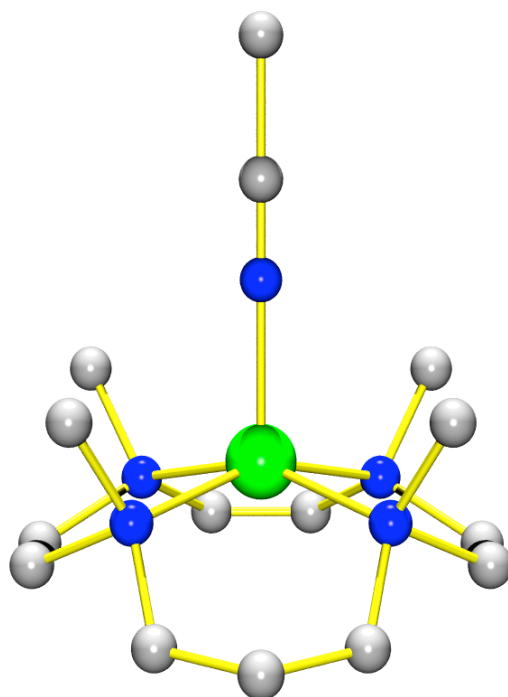The 3d1u was not considered since there is no literature precedent for this orientation.

[b]Same representation as Table S3.
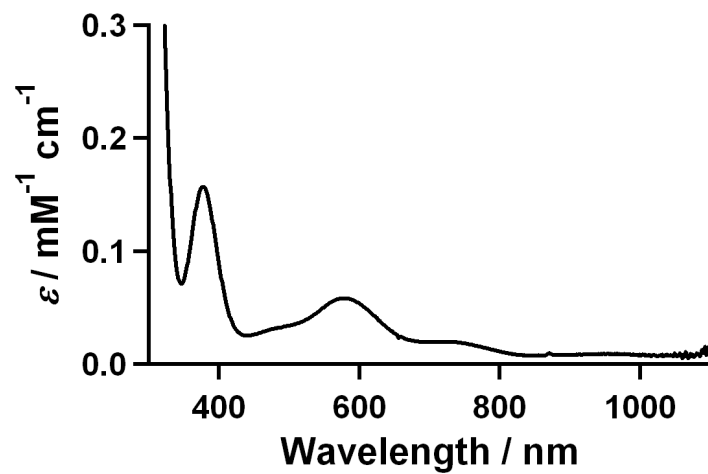
Fig. S1. UV-vis spectrum of $[Ni^{II}(13\text{-TMC})(CH_3CN)]^{2+}$ (**1**) in CH_3CN at 25 $^{\circ}$C.

Fig. S2. ESI-MS spectrum of $[Ni^{II}(13\text{-}TMC)(CH_3CN)]^{2+}$ (**1**) in CH_3CN at 25 °C. Mass peaks at 150.2, 170.3, and 399.3 are assigned to $[Ni^{II}(13\text{-}TMC)]^{2+}$, $[Ni^{II}(13\text{-}TMC)(CH_3CN)]^{2+}$, and $[Ni^{II}(13\text{-}TMC)(ClO_4)]^{+}$, respectively.

Fig. S3. X-ray crystal structure of $[Ni^{II}(13\text{-}TMC)(CH_3CN)]^{2+}$ (**1**) (gray C, blue N, green Ni).
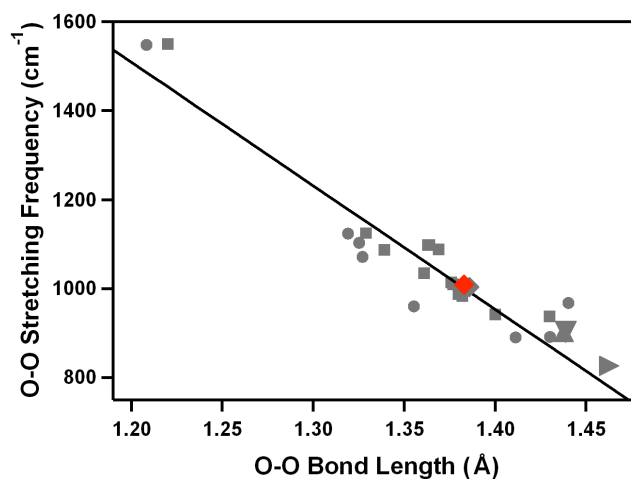
Fig. S4. Plot of O-O stretching frequency (cm^{-1}) vs O-O bond distance (Å) for side-on metal-O_2 complexes. Gray points represent experimental and theoretical data previously reported (J. Cho et al, *Acc. Chem. Res*. 2012, **45**, 1321-1330). The solid line represents a least-squares linear fit of the experimental and theoretical data. $[Ni^{III}(13\text{-}TMC)(O_2)]^+$ (**3**) (◆) is included in the diagram.
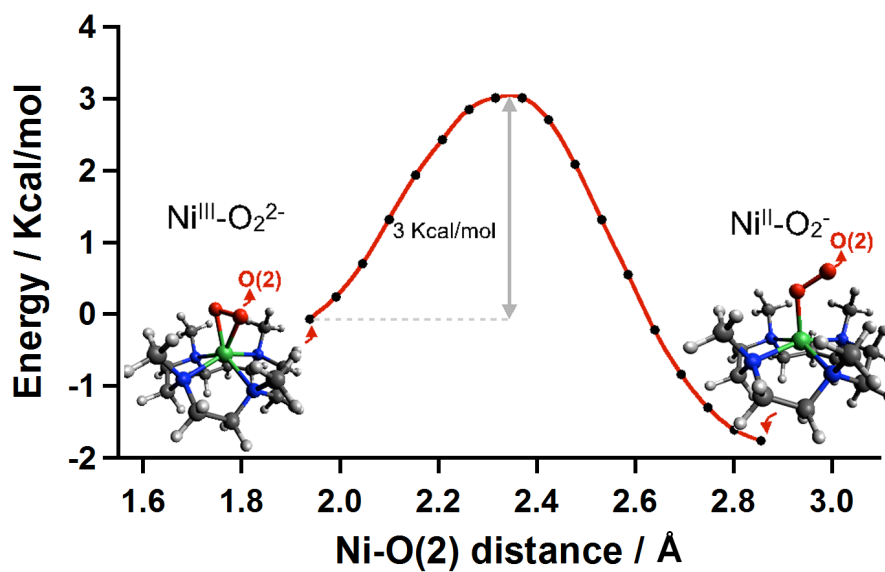
Fig. S5. DFT calculated interconversion energy for $[Ni^{II}(13\text{-}TMC)(O_2)]^+$ (**2**) and $[Ni^{III}(13\text{-}TMC)(O_2)]^+$ (**3**). The energy diagram was calculated by varying the Ni-O(2) distance from 1.903 (fully optimized distance in **3**) to 2.837 (fully optimized distance in **2**) Å. The same DFT protocol was used as for the interconversion energy calculation as used for the geometry optimizations.